HEFAT2014
10th International Conference on Heat Transfer, Fluid Mechanics and Thermodynamics
14 – 26 July 2014
Orlando, Florida

ALKALINE MEMBRANE FUEL CELL (AMFC) STACK MODELING AND SIMULATION

Vargas J.V.C.*, Polla P.T.B., Balmant W. and Ordonez J. C.
*Author for correspondence
Department of Mechanical Engineering,
Federal University of Parana,
Curitiba,
Brazil,
E-mail: vargasjvcv@gmail.com

ABSTRACT

This paper aims to produce a dynamic model that is computationally fast to predict the response of the AMFC stack according to variations of physical properties of the materials, and operating and design parameters. The model is based on electrochemical principles, and mass, momentum, energy and species conservation. It also takes into account pressure drop in the headers, single cells gas channels and the temperature gradient with respect to space in the flow direction. The simulation results comprise temperature distribution, net power, polarization and efficiency curves. Therefore, the model is expected to be a useful tool for AMFC stack control, design and optimization purposes after adjustment and experimental validation.

INTRODUCTION

The technology of fuel cells has been widely studied as an alternative renewable energy in order to contribute to solve the problem of the world energy demand increase, and it is considered a form of clean energy generation [1-8]. The fuel cell operates through an electrochemical reaction between a fuel and an oxidant, producing energy and water [2]. In the case of the alkaline membrane fuel (AMFC) hydrogen is used as fuel, oxygen as oxidant and an aqueous solution of potassium hydroxide (KOH) supported by a cellulose membrane as the electrolyte, and platinum or platinum free (e.g., Ni-Co) based catalysts in the electrodes.

Despite its advantages, fuel cell technology is still not widely used because there are obstacles to be overcome, such as the high cost of catalysts and manufacturing, difficulty in hydrogen production as well as its storage and distribution [1,2]. The alkaline membrane fuel cell (AMFC) is an alternative to reduce cost, compared to the proton exchange membrane fuel cell (PEMFC).

Much attention has been given to modeling fuel cell systems. Such efforts include the fluid flows that supply the cells with fuel and oxidant, with the use of computational fluid dynamics (CFD), as described by [3, 4], who reviewed the status of three-dimensional fuel cell modelling.

Sommer et al. [5] developed a mathematical model for the single AMFC, where the simulation results comprise temperature distribution, net power and polarization curves. The model was experimentally validated.

For practical engineering applications, stacks are necessary to reach higher power output. Vargas et al. [9] conducted a study to optimize the internal structure, single cells thickness, and the external shape of a PEMFC stack, so that net power is maximized. For that, the authors started from a mathematical model of a single fuel cell in the stack, proceeding to include the pressure drop experienced in the headers, and the gas channels of the cells.

This paper extends the mathematical model and the numerical simulation of a single AMFC to alkaline membrane fuel cell (AMFC) stacks. Pressure drops in the headers and single cells channels are included in order to assess the AMFC stack net power output.

MATHEMATICAL MODEL

The AMFC stack is shown schematically in Figure 1. The stack is fed by two input headers, one carries fuel and the other carries oxidant, which are delivered individually to each fuel cell inside the stack. After the fuel and oxidant flows cross each cell in the stack, two output headers collect the used gases, and water which is produced by the reactions in the fuel cells. The stack produces electrical power, and a fraction of this energy is used to pump the fuel and oxidant across the AMFC stack, through the input and output headers and also through the gas channels in each cell. The model considers pure hydrogen as the fuel and oxygen as the oxidant.

The single AMFC is divided into seven control volumes that interact energetically with one another and the external ambient. The model assumes the existence of a cooling channels system that irrigates the bipolar plates, and the cooling fluid (e.g., water, air) is kept at an average specified temperature, T_∞, between single cells, and around the stack.

NOMENCLATURE

A	[m^2]	area
A_c	[m^2]	total gas channel cross-section area
A_s	[m^2]	fuel cell cross-section area
A_w	[m^2]	wall heat transfer area
AFC		alkaline fuel cell
AMFC		alkaline membrane fuel cell
B		dimensionless constant
C		constant
C_i	[mol/m^3]	concentration of oxidized and reduced states, i=O,R
CFD		computational fluid dynamics
CV_i		control volume i
c	[Kmol/kgK]	specific heat
c_p	[kJ/kgK]	specific heat at constant pressure
c_v	[kJ/kgK]	Specific heat at constant volume
D	[m^2/s]	Knudsen diffusion coefficient
D_h	[m]	gas channel hydraulic diameter
f		friction factor
F	[96,500C/eq]	Faraday constant
h	[W/m^{2}K]	heat transfer coeficient
$H_i(T_i)$	[kJ/kmol]	molar enthalpy of formation at temperature T_i of reactants and products
$\tilde{H}_i(\theta_i)$	[kJ/kmol]	dimensionless molar enthalpy of formation at temperature Θ_i of reactants and products of compound i
$i_{o,a}$, $i_{o,c}$	[A/m^2]	anode and cathode exchange current densities
$i_{Lim,a}$,$i_{Lim,c}$	[A/m^2]	anode and cathode limiting current densities
I	[A]	current
j	[kgm^2/s]	mass flux
k	[W/mK]	thermal conductivity
$k°$	[m/s]	standard rate constant
K	[m^2]	permeability
L	[m]	length
L_c,L_t	[m]	gas channels internal dimensions
L_x, L_y, L_z	[m]	stack length, width and height, respectively
m	[kg]	mass
$\dot{m}$	[kg/s]	mass flow rate
M	[kg/kmol]	molecular weight
n	[eq/mol]	equivalent electron per mole of reactant
$\dot{n}$	[mol/s]	molar flow rate
N		dimensionless global wall heat transfer coefficient
n_c		number of parallel ducts in gas channel
p	[N/m^2]	pressure
P		dimensionless pressure
p_a		precision limit of quantity a
p_s	[m]	perimeter of cross-section
PEMFC		proton exchange membrane fuel cell
Pr	$\mu c_p/k$	Prandtl number
q		tortuosity
Q		reaction quotient
$\dot{Q}$	[W]	heat transfer rate
r	[m]	pore radius
R	[kJ/kgK]	ideal gas constant
$\bar{R}$	[8,314kJ/kgK]	universal gas constant
Re_{D_h}	$uD_h\rho/\mu$	Reynolds number based on D_h
t	[s]	time
T	[K]	temperature
u	[m/s]	mean velocity
U		global wall heat transfer coefficient
U_a		uncertainty of quantity a
V	[V]	electrical potential
V_T	[m^3]	total volume
y		electrolyte solution mass fraction
W	[J]	electrical work
$\dot{W}$	[W]	electrical power
$\tilde{W}$		dimensionless fuel cell electrical power
$\tilde{W}_{net}$		dimensionless fuel cell net power
$\tilde{W}_p$		dimensionless required pumping power
[.]	[mol/l]	molar concentration of a substance

Greek Symbols

α		charge transfer coefficient
β	[Ω]	electrical resistance
γ		ratio of specific heats
δ		gas channel aspect ratio
ΔG	[kJ/kmol H_2]	molar Gibbs free energy change
ΔH	[kJ/kmol H_2]	molar enthalpy change
ΔP		dimensionless pressure drop in gas channels
ΔS	[kJ/kmol]	molar entropy change
ΔT	[K]	temperature change
ζ		stoichiometric ratio
η_a, η_c	[V]	anode and cathode charge transfer overpotentials
$\eta_{d,a}$, $\eta_{d,c}$	[V]	anode and cathode mass diffusion overpotentials
η_{ohm}	[V]	fuel cell total ohmic potential loss
Θ		dimensionless temperature
μ	[kg/ms]	viscosity
ν_i		reaction coefficient
ξ		dimensionless length
ρ	[kg/m^3]	density
σ	[1/ Ωm]	electrical conductivity
τ		dimensionless time
ϕ		porosity
ψ		dimensionless mass flow rate

Subscripts

a	anode
(aq)	aqueous solution
c	channel or cathode
cel	solid part of electrolyte
dif	diffusion
e	reversible
f	fuel
(g)	gaseous phase
H_2	hydrogen
H_2O	water
i	substance or location in AMFC
i	irreversible
i,a	irreversible at the anode
i,c	irreversible at the cathode
j	location in AMFC
KOH	potassium hydroxide
(l)	liquid phase
max	maximum
memb	electrolyte membrane (solid and liquid parts)
ohm	ohmic
opt	optimal
ox	oxidant
OH^-	hydroxide ion
O_2	oxygen
ref	reference level
s,a	anode solid part
s,c	cathode solid part
s	solid phase; single cell thickness
sol	electrolyte solution
w	wall
wet	wetted
0	nitial condition
1,…,7	control volumes
12	interaction between CV1 and CV2
23	interaction between CV2 and CV3
34	interaction between CV3 and CV4
45	interaction between CV4 and CV5
56	interaction between CV5 and CV6
67	interaction between CV6 and CV7
∞	ambient

Superscript

°	standard conditions [gases at 1 atm, 25ºC, species in solution at 1 M, where M is the molarity = [(moles solute)/(liters solution)]
~	dimensionless variable

The total AMFC stack electrical power output results from the analysis of a single cell, which is the electrical power produced by a single AMFC multiplied by the number of cells in the stack. However, the required pumping power depends on the flow structure of the entire AMFC stack.

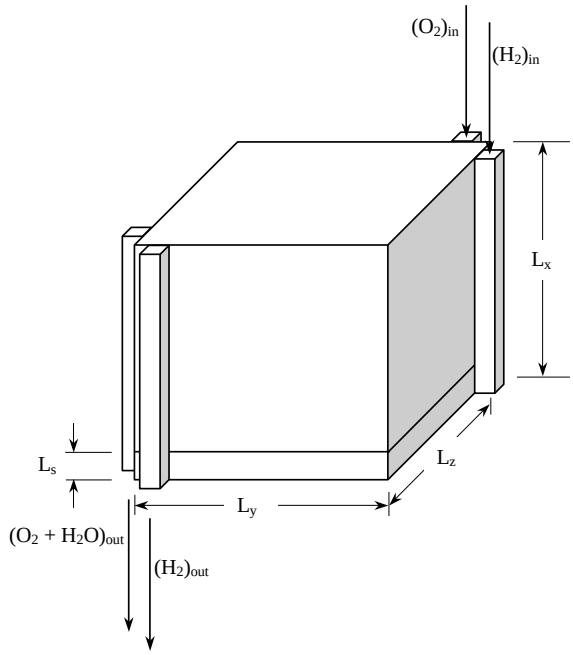

Figure 1 The configuration of the AMFC stack

The mathematical model for a single AMFC was introduced in a previous study by Sommer et al. [5]. However, significant changes need to be implemented in the single cell model so that the stack response could be assessed.

The single AMFC is divided in seven control volumes as shown in Figure 2, i.e.: fuel channel (CV1), anode diffusion layer (CV2), anode reaction layer (CV3), alkaline cellulose membrane (CV4), cathode reaction layer (CV5), cathode diffusion layer (CV6), and oxidant gas channel (CV7).

The model consists of writing mass, energy and species conservation equations for each control volume, considering the chemical reactions on CV3 and CV5. All flow phenomena are considered, resulting on a time dependent internal flow model. It takes into consideration, in the balance of energy, the heat generated by the electrochemical reactions, and the potential losses. The heat generation is due to the heat of reaction, ohmic resistance throughout the fuel cell, and also by the activation and diffusion overpotential losses in CV3 and CV5.

The solution of the differential and algebraic equations produces temperature and pressure profiles for each control volume, and polarization and power curves. The actual electric potential is obtained by subtracting the all overpotential losses from the reversible potential, i.e., activation (on the reaction kinetics), ohmic (electronic and ionic resistances) and concentration (mass transport). Such values are functions of the potential of the fuel cell or the total current (I), which have a one-to-one relationship with each other. Once the external load determines the operating current of the fuel cell, in this work the total current of the cell is regarded as the independent variable. For the sake of generality, and for control and real time operation, a dynamic analysis is conducted.

The problem variables, i.e., volume, temperature, pressure, mass flow rates, wall global heat transfer coefficient, heat transfer coefficients, thermal conductivities, areas, specific heats and time, were nondimensionalized in order to obtain a normalized solution to any possible AMFC stack architecture.

The hydrogen mass flow rate results from a current (I), required by the external load as follows:

$$\dot{m}_{H_2} = \dot{n}_{H_2} M_{H_2} = \frac{I}{nF} M_{H_2} \qquad (1)$$

where $\dot{n}$ is the molar flow rate, M is the molecular weight, n is the equivalent electron per mole of reactant, I is the total current, and F is the Faraday constant. The mass flow of oxygen necessary for a single AMFC is $\dot{m}_{O_2} = 1/2\dot{n}_{H_2} M_{O_2}$ and so $\dot{n}_{O_2} = \dot{n}_{H_2}$.

The fuel (hydrogen) enters CV1, and the oxidant (oxygen) enters CV7. This is seen in Figure 2. A balance of mass and energy applied to the CV1 states that:

$$\frac{d\theta_1}{d\tau} = \left[\tilde{Q}_{w1} + \psi_f\left(\theta_f - \theta_1\right) + \tilde{Q}_{12} + \tilde{Q}_{1ohm}\right] \frac{\theta_{1,0}\gamma_f}{P_f n_c \xi_1 \xi_c \xi_z} \qquad (2)$$

where θ is the dimensionless temperature, $\tilde{Q}_i = \dot{Q}_i / \dot{m}_{ref} c_{p,f} T_\infty$ the dimensionless heat transfer rate, $\tilde{Q}_{12} = \tilde{h}_1 \tilde{A}_s (1 - \phi_2)(\theta_2 - \theta_1)$, $\tilde{Q}_{wi} = N_i \tilde{A}_{wi}(1 - \theta_i)$, $\tilde{Q}_{iohm} = I^2 \beta_i / \left(\dot{m}_{ref} c_{p,f} T_\infty\right)$, β the electrical resistance, $\theta_{i,0}$ the initial condition, ϕ the porosity, $\tilde{A}_s = L_y L_z / V_T^{2/3}$, $\psi_f = \zeta_1 \psi_{H_2}$, and ζ the stoichiometric ratio which is assumed greater than 1 on both sides.

The pressure drops in the gas channels, from the input headers to the output headers, are given by the pressure drops in a single cell only, because they are in parallel, as shown in Figure 3. The resulting dimensionless expression for rectangular shaped gas channels, accounting for the flow directional change (90º at the cell inlet and outlet), contraction (inlet) and expansion (outlet), together with the ideal gas model, is the following:

$$\Delta P_i = \left[f_i \left(\frac{\xi_z}{\xi_i} + \frac{\xi_z}{\xi_c} \right) + \frac{K_{bc}}{2} + \frac{K_{be}}{2} \right] \frac{P_j}{\theta_i} \frac{R_f}{R_j} \tilde{u}_i^2 \qquad (3)$$

where i = 1, 7 and j = f, ox, respectively. Here $\tilde{u}_i = \left(\tilde{u}_{i,in} + \tilde{u}_{i,out}\right)/2$ is the gas dimensionless mean velocity in the channel, defined as $\tilde{u} = u/\left(R_f T_\infty\right)^{1/2}$, f is the friction factor, K_{bc} and K_{be} are the bending-contraction and bending-expansion coefficients, respectively. According to mass conservation, the flow dimensionless mean velocities in the gas channels are $\tilde{u}_1 = C\theta_1 \left(\psi_f - \psi_{H_2}/2\right) / \left(\tilde{A}_{c1} P_f\right)$, $\tilde{u}_7 = R_{ox} C\theta_7 \left(\psi_{ox} - \psi_{O_2}/2\right)$

$/\left(R_f \tilde{A}_{c7} P_{ox}\right)$, where $C = \left(R_f T_\infty\right)^{1/2} \dot{m}_{ref} / \left(p_\infty V_T^{2/3}\right)$, and $\tilde{A}_{ci} = n_c L_c L_i / V_T^{2/3}$, i = 1, 7, is the dimensionless total duct cross section area in the fuel and oxidant channels, respectively.

The model also requires the evaluation of the friction factor and heat transfer coefficients in the gas channels. For the laminar regime ($Re_{D_h} < 2300$), the following correlations are used [10]: $f_i Re_{D_{h,i}} = 24\left(1 - 1.3553\delta_i + 1.9467\delta_i^2 - 1.7012\delta_i^3 + 0.9564\delta_i^4 - 0.2537\delta_i^5\right)$; $\frac{h_i D_{h,i}}{k_i} = 7.541\left(1 - 2.610\delta_i + 4.970\delta_i^2 - 5.119\delta_i^3 + 2.702\delta_i^4 - 0.548\delta_i^5\right)$, where $\delta_i = L_c / L_i$, for $L_c \le L_i$ and $\delta_i = L_i / L_c$, for $L_c > L_i$; $D_{h,i} = 2L_cL_i/(L_c + L_i)$, $Re_{D_{h,i}} = u_i D_{h,i}\rho_i/\mu_i$ and i = 1, 7. The correlations used for the turbulent regime were [11] $f_i = 0.079 Re_{D_h}^{-1/4}$ $(2300 < Re_{D_{h,i}} < 2 \times 10^4)$; $f_i = 0.046 Re_{D_h}^{-1/5}$ $(2\times10^4 < Re_{D_{h,i}} < 10^6)$, for friction, and $\frac{h_i D_{h,i}}{k_i} = \frac{(f_i/2)\left(Re_{D_{h,i}} - 10^3\right)Pr_i}{1 + 12.7\left(f_i/2\right)^{1/2}\left(Pr^{2/3} - 1\right)}$, for heat transfer with $(2300 < Re_{D_{h,i}} < 5 \times 10^6)$, where Pr is the gas Prandtl number, $\mu c_p/k$.

The overall fuel cell reaction and the mass balance for CV7 yield $\dot{n}_{H_2O} = \dot{n}_{H_2O,out} = \dot{n}_{H_2O,in} = \dot{n}_{O_2}$. Therefore, the mass and energy balances for CV7 state that:

$$\frac{d\theta_7}{d\tau} = \left[\tilde{Q}_7 + \tilde{H}_{H_2O}(\theta_6) - \tilde{H}_{H_2O}(\theta_7) + \psi_{ox}\frac{c_{p,ox}}{c_{p,f}}(\theta_{ox} - \theta_7)\right]\frac{R_{ox}}{R_f}\frac{\gamma_{ox}\theta_{7,0}}{P_{ox}n_c\xi_c\xi_7\xi_z} \quad (4)$$

where $\tilde{Q}_7 = -\tilde{Q}_{67} + \tilde{Q}_{w7} + \tilde{Q}_{7ohm}$, $\tilde{Q}_{67} = \tilde{h}_7\tilde{A}_s(1 - \phi_6)(\theta_7 - \theta_6)$, and the dimensionless enthalpy of formation is defined as $\tilde{H}_i = \dot{n}_i H_i / \left(\dot{m}_{ref} c_{p,f} T_\infty\right)$, in which the subscript i refers to a substance or a control volume.

Hydrogen diffuses through CV1 and CV3, and oxygen and water vapor diffuse through CV5, CV6 and CV7. Therefore, the mass and energy balance for CV2 state that:

$$\frac{d\theta_2}{d\tau} = \left[(\theta_1 - \theta_2) + \frac{\tilde{Q}_2}{\psi_{H_2}}\right]\frac{\gamma_{s,a}\psi_{H_2}}{\rho_{s,a}(1-\phi_2)\xi_2\xi_y\xi_z} \quad (5)$$

where $\tilde{Q}_2 = -\tilde{Q}_{12} + \tilde{Q}_{w2} + \tilde{Q}_{23} + \tilde{Q}_{2ohm}$, $\tilde{Q}_{23} = \tilde{k}_{s,a}(1 - \phi_2)\tilde{A}_s(\theta_2 - \theta_3)/[(\xi_2 + \xi_3)/2]$, $\tilde{\rho}_i = \rho_i R_f T_\infty / p_\infty$, $\gamma_{s,a} = c_{p,f}/c_{v,s,a}$, and the subscript s,a and s,c mean the solid part of the anode and cathode, respectively.

The mass balance for CV6, yields $\dot{m}_{O_{2,out}} = \dot{m}_{O_{2,in}} = \dot{m}_{O_2}$ and $\dot{n}_{H_2O} = \dot{n}_{H_2O,out} = \dot{n}_{H_2O,in} = \dot{n}_{O_2}$. The mass and energy balances for CV6 state that:

$$\frac{d\theta_6}{d\tau} = \left[\tilde{Q}_6 + \psi_{O_2}\frac{c_{p,ox}}{c_{p,f}}(\theta_7 - \theta_6) + \tilde{H}_{H_2O}(\theta_5) - \tilde{H}_{H_2O}(\theta_6)\right]\frac{\gamma_{s,c}}{\rho_{s,c}(1-\phi_6)\xi_6\xi_y\xi_z} \quad (6)$$

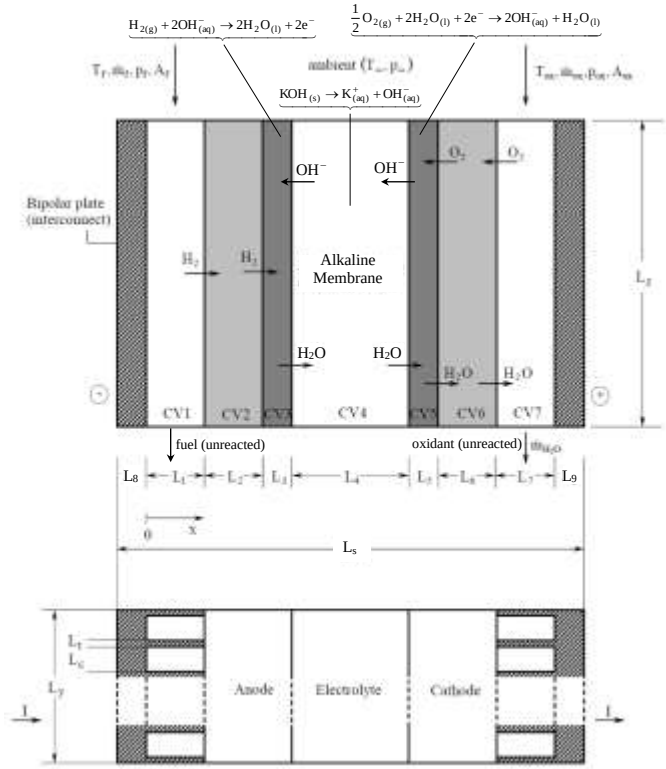

Figure 2 The internal structure of a single AMFC

where $\tilde{Q}_6 = -\tilde{Q}_{56} + \tilde{Q}_{w6} + \tilde{Q}_{67} + \tilde{Q}_{6ohm}$, $\tilde{Q}_{56} = \tilde{k}_{s,c}(1 - \phi_6)\tilde{A}_s(\theta_5 - \theta_6)/[(\xi_5 + \xi_6)/2]$, and $\gamma_{s,c} = c_{p,f}/c_{v,s,c}$.

Diffusion is assumed to be the dominant mass transfer mechanism in the diffusion and catalytic layers. As the friction of the substances with the pore walls is considered, the Knudsen flow is used to represent the fuel and oxidant mass flow [5], i.e., $j_i = -\left[D\left(\rho_{out} - \rho_{in}\right)/L\right]_i$, $i = 2,6$, where the Knudsen diffusion coefficient is $D = B \cdot \left[r \cdot \left(\frac{8\overline{R}T}{\pi M}\right)^{1/2} \cdot \phi^q\right]$, r the pore radius, ρ the density, $\overline{R}$ the universal gas constat, M the gas molecular weight, ϕ the porosity, q the tortuosity [5], and B a dimensionless coefficient.

The output pressure of the diffusive layer, which is equal to the input pressure of the catalyst layer, is obtained using the ideal gas model, i.e., $P_{i,out} = P_{i,in} - \frac{j_i R_i T_\infty L_i \theta_i}{D_i p_\infty}$ $i = 2,6$, where $j_2 = \dot{m}_{H_2} / A_{3,wet}$ and $j_6 = \dot{m}_{O_2} / A_{5,wet}$, and $A_{3,wet}$ and $A_{5,wet}$ are the wetted areas in the porous catalyst layers. Note also that $P_{2,in} = P_f$ and $P_{6,in} = P_{ox}$. The average pressures in CV2 and CV6 are estimated as $P_i = \frac{1}{2}\left(P_{i,in} + P_{i,out}\right)$, $i = 2,6$

The wetted areas in the porous catalyst layers $A_{3,wet}$ and $A_{5,wet}$ are estimated by considering dual-porosity sintered metal electrodes, in which the average pore diameter is considered to be roughly the same order as the square root of the porous medium permeability [1]. In this consideration the pores are approximated as parallel tubes, i.e., $A_{j,wet} = \left\{4\phi_j L_j K_j^{-1/2} + \left(1-\phi_j\right)\right\} A_s$.

CV3 is formed by the porous electrode, the fuel (hydrogen), and the electrolyte solution (KOH) that is present in the pores of the electrode. The electrons released by the oxidation of hydrogen in CV3 pass through an external circuit and participate in the reduction of oxygen in CV5. CV5 contains a porous electrode, oxygen and electrolyte solution. The hydrogen oxidation reaction (HOR) and oxygen reduction reaction (ORR) are written as follows:

$$H_{2(g)} + 2OH^-_{(aq)} \rightarrow 2H_2O_{(l)} + 2e^- \quad (7)$$

$$\frac{1}{2}O_{2(g)} + 2H_2O_{(l)} + 2e^- \rightarrow 2OH^-_{(aq)} + H_2O_{(l)} \quad (8)$$

In CV3 and CV5, the mass of liquid contained in these control volumes is considered negligible compared to the solid mass of the electrode. CV3 and CV5 interact thermally with the adjacent control volumes by conduction, and with the ambient by convection, and generate heat through chemical reactions and irreversible mechanisms (ohmic resistance, activation and concentration overpotential losses).

Sommer et al. [5] included heat generation due to losses by activation overpotential (η_a) and concentration ($\eta_{d,a}$), which had not been considered in the study of Vargas and Bejan [1].

The mass and energy balance for CV3 result in $\dot{n}_{H_2} = \dot{m}_f/M_{H_2}$, $\dot{n}_{H_2O} = 2\dot{n}_{H_2}$, $\dot{m}_{H_2O} = 2\dot{n}_{H_2}M_{H_2O}$, $\dot{n}_{OH^-} = 2\dot{n}_{H_2}$, $\dot{m}_{OH^-} = 2\dot{n}_{H_2}M_{OH^-}$ and

$$\frac{d\theta_3}{d\tau} = \left[\tilde{Q}_3 - \Delta\tilde{H}_3 + \Delta\tilde{G}_3\right]\frac{\gamma_{s,a}}{\rho_{s,a}(1-\phi_3)\xi_3\xi_y\xi_z} \quad (9)$$

where, $\tilde{Q}_{3,act} = \eta_a I/\left(\dot{m}_{ref}c_{p,f}T_\infty\right)$, $\tilde{Q}_{3,dif} = \eta_{d,a}I/\left(\dot{m}_{ref}c_{p,f}T_\infty\right)$, $\tilde{Q}_3 = -\tilde{Q}_{23} + \tilde{Q}_{w3} + \tilde{Q}_{34} + \tilde{Q}_{3ohm} + \tilde{Q}_{3,act} + \tilde{Q}_{3,dif}$, and $\tilde{Q}_{34} = -(1-\phi_3)(\theta_3-\theta_4)2\tilde{A}_s k_{s,a}k_{memb}/\left(\xi_4 k_{s,a} + \xi_3 k_{memb}\right)$.

Analogously, the mass and energy balance are applied to CV5, considering the chemical reactions $\dot{n}_{H_2O,in} = 2\dot{n}_{H_2O,out} = \dot{n}_{O_2}$, $\dot{n}_{OH^-_{out}} = 2\dot{n}_{O_2}$, so that

$$\frac{d\theta_5}{d\tau} = \left[\tilde{Q}_5 - \Delta\tilde{H}_5 + \Delta 5\right]\frac{\gamma_{s,c}}{\rho_{s,c}(1-\phi_5)\xi_5\xi_y\xi_z} \quad (10)$$

where, $\tilde{Q}_{5,act} = \eta_c I/\left(\dot{m}_{ref}c_{p,f}T_\infty\right)$, $\tilde{Q}_{5,dif} = \eta_{d,c}I/\left(\dot{m}_{ref}c_{p,f}T_\infty\right)$, $\tilde{Q}_5 = -\tilde{Q}_{45} + \tilde{Q}_{w5} + \tilde{Q}_{56} + \tilde{Q}_{5ohm} + \tilde{Q}_{5,act} + \tilde{Q}_{5,dif}$, and $\tilde{Q}_{45} = -(1-\phi_5)(\theta_4-\theta_5)2\tilde{A}_s k_{s,c}k_{memb}/\left(\xi_4 k_{s,c} + \xi_5 k_{memb}\right)$.

The AMFC electrolyte consists of a KOH alkaline solution supported by a solid inert cellulose membrane (paper). Equations (7) and (8) and the conservation of mass in CV4 require that $2\dot{n}_{H_2} = \dot{n}_{OH^-,out} = \dot{n}_{OH^-,in} = 2\dot{n}_{O_2}$, $2\dot{n}_{H_2} = \dot{n}_{H_2O,in} = \dot{n}_{H_2O,out} = 2\dot{n}_{O_2}$. In CV4, the mass of fluid cannot be neglected in the thermal analysis, therefore the balance of energy applied to CV4 results in

$$\frac{d\theta_4}{d\tau} = \left[\tilde{Q}_4 + \tilde{H}_{OH^-}(\theta_5) - \tilde{H}_{OH^-}(\theta_4) + \tilde{H}_{H_2O}(\theta_3) - \tilde{H}_{H_2O}(\theta_4)\right]\frac{\gamma_{memb}}{\rho_{memb}\xi_4\xi_y\xi_z} \quad (11)$$

where $\tilde{Q}_4 = -\tilde{Q}_{34} + \tilde{Q}_{w4} + \tilde{Q}_{45} + \tilde{Q}_{4ohm}$, $\rho_{memb} = \rho_{sol}\phi_4 + \rho_{cel}(1-\phi_4)$, $c_{p,memb} = c_{p,sol}\phi_4 + c_{p,cel}(1-\phi_4)$, and $k_{memb} = k_{sol}\phi_4 + k_{cel}(1-\phi_4)$.

Based on the electrical conductivities and geometry of each compartment, the electrical and ionic resistance, β (Ω), are given by:

$$\beta_i = \frac{\xi_i}{\tilde{A}_s V_T^{1/3}\sigma_i(1-\phi_i)}, \; i = 1,2,6,7 \; (\phi_1, \phi_7 = 0) \quad (12)$$

$$\beta_i = \frac{\xi_i}{\tilde{A}_s V_T^{1/3}\sigma_i\phi_i}, \quad i = 3,4 \; e \; 5 \quad (13)$$

For i = 3, 4, and 5, $\sigma_i = \sigma_{sol}$. The conductivities of the diffusive layer (σ_2) and (σ_6) are the conductivities of the electrode carbon phases, and (σ_1) and (σ_7) are given by the electrical conductivity of the bipolar plates material.

The dimensionless potential and overpotentials are nondimensionalized with respect to a reference potential V_{ref}, so that $\tilde{V}_i = V_i/V_{ref}$ and $\tilde{\eta}_i = \eta_i/V_{ref}$.

The actual potential $\left(\tilde{V}_i\right)$ supplied by a fuel cell results from the combination between the irreversible potential of the anode $\left(\tilde{V}_{i,a}\right)$, irreversible potential of the cathode $\left(\tilde{V}_{i,c}\right)$ and ohmic loss $(\tilde{\eta}_{ohm})$, which occurs all across the fuel cell between CV1 and CV7, as follows :

$$\tilde{V}_i = \tilde{V}_{i,a} + \tilde{V}_{i,c} - \tilde{\eta}_{ohm} \quad (14)$$

$$\tilde{\eta}_{ohm} = \frac{I}{V_{ref}}\sum_{i=1}^{7}\beta_i \quad (15)$$

In order to estimate the available power provided by a fuel cell $\left(\widetilde{W}_{net}\right)$, it is necessary to subtract the pumping power necessary to supply the fuel cell with fuel and oxidant $\left(\widetilde{W}_p\right)$ from the total power produced by the cell. Therefore, the AMFC stack net power output is given by:

$$\widetilde{W}_{net} = \widetilde{W} - \widetilde{W}_p \quad (16)$$

where, $\widetilde{W} = \tilde{V}_i\tilde{I}$ is the total electric power produced by the fuel cell. The dimensionless pumping power $\widetilde{W}_p$ is given by:

$$\widetilde{W}_p = \psi_f S_f \frac{\theta_i}{P_i}\Delta P_1 + \psi_{ox}S_{ox}\frac{\theta_7}{P_7}\Delta P_7 \quad (17)$$

where, $S_i = \dot{m}_{ref}T_\infty R_i/V_{ref}I_{ref}$, $i = f, ox$.

Next, the pressure drops in the input and output headers are calculated according to the schematic diagram presented in Figure 3. In the input headers, the mass flow rates of fuel and oxidant, $\psi_{f,in} = n_s\psi_f$ and $\psi_{ox,in} = n_s\psi_{ox}$, supply each single cell level with fuel and oxidant mass flow rates, ψ_f and ψ_{ox}, respectively. Therefore, the model assumes that the mass flow rates in the headers are distributed evenly to each single cell. In the output headers, each single cell delivers depleted fuel and oxidant mass flow rates, and the water mass flow rate produced by the electrochemical reaction, $(\zeta_1 - 1)\psi_f$, $(\zeta_7 - 1)\psi_{ox}$, and ψ_{H_2O}, respectively. Therefore, the fuel, oxidant and water mass flow rates in the headers vary according to each single cell level, and so do the flow mean velocities. As a result, the fuel and oxidant pressure drops in each segment of the headers adjacent to a single cell level "i", and the water flow pressure drop in the oxidant output header are calculated by

$$\Delta P_{i,k} = f_{i,k}\left(\frac{\xi_s}{\xi_v} + \frac{\xi_s}{\xi_h}\right)\frac{P_j}{\theta_{i,k}}\frac{R_f}{R_j}\tilde{u}_{i,k}^2 \quad (18)$$

$$\Delta P_{wa,i} = f_i\left(\frac{\xi_s}{\xi_v} + \frac{\xi_s}{\xi_h}\right)\tilde{\rho}_{wa}\tilde{u}_{wa,i}^2 \quad (19)$$

where $k = h_{f,in}, h_{ox,in}, h_{f,out}, h_{ox,out}$ represents the fuel input headers (f) and oxidants (ox), fuel output headers and oxidant, respectively. In equations (18) and (19), in the input headers the temperatures are the known inlet fuel and oxidant temperatures, and in the output headers, the temperatures are temperatures of the fuel and oxidant exiting the single cell, calculated by the model, i.e., θ_1 and θ_7, respectively. Here $\tilde{u}$ is the dimensionless mean velocity, f is the friction factor calculated for laminar flow, with $\delta_i = L_h / L_v$, for $L_h \le L_v$ and $\delta_i = L_v / L_h$, for $L_h > L_v$; $D_{h,i} = 2L_hL_v/(L_h + L_v)$, or for the turbulent flow regimes, as described previously in the text.

According to mass conservation, the dimensionless gas mean velocities in the headers at each single cell level "i" in the stack are given by $\tilde{u}_{i,k} = C[R\theta\psi/(\phi P)]_{i,k}/(R_f\tilde{A}_{ch})$, and for the water in the oxidant output header, $\tilde{u}_{wa,i} = C\psi_{wa,i}\left[\tilde{\rho}_{wa}\left(1-\phi_{i,h_{ox,out}}\right)\tilde{A}_{ch}\right]$, where k = $h_{f,in}$, $h_{ox,in}$, $h_{f,out}$, $h_{ox,out}$ represent the input fuel and oxidant headers, output fuel and oxidant headers; $\tilde{A}_{ch} = L_hL_v / V_T^{2/3}$, is the dimensionless cross section area in the fuel and oxidant headers; $\phi_{i,k} = 1$ for all headers, except in the oxidant output header, when $\phi_{i,k} < 1$ since oxidant and water flow in the header.

Additional power is required to pump fuel, oxidant and produced water to in and out of the headers shown in Figure 3. The dimensionless pumping power required for the gases at the fuel cell level *i*, and to the produced water out of the oxidant output headers, are given by:

$$\widetilde{W}_{i,k} = S_j\left[\frac{\psi\theta\Delta P}{P}\right]_{i,k}, \; j = f, ox \quad (20)$$

$$\widetilde{W}_{wa,i} = \frac{S_f}{\tilde{\rho}_{wa}}[\psi\Delta P]_{wa,i} \quad (21)$$

The total AMFC stack power available to use is therefore obtained from

$$\widetilde{W}_{net} = n_s(\widetilde{W}_s - \widetilde{W}_p) - \sum_k\sum_{i=1}^{n_s}\widetilde{W}_{i,k} - \sum_{i=1}^{n_s}\widetilde{W}_{wa,i} \quad (22)$$

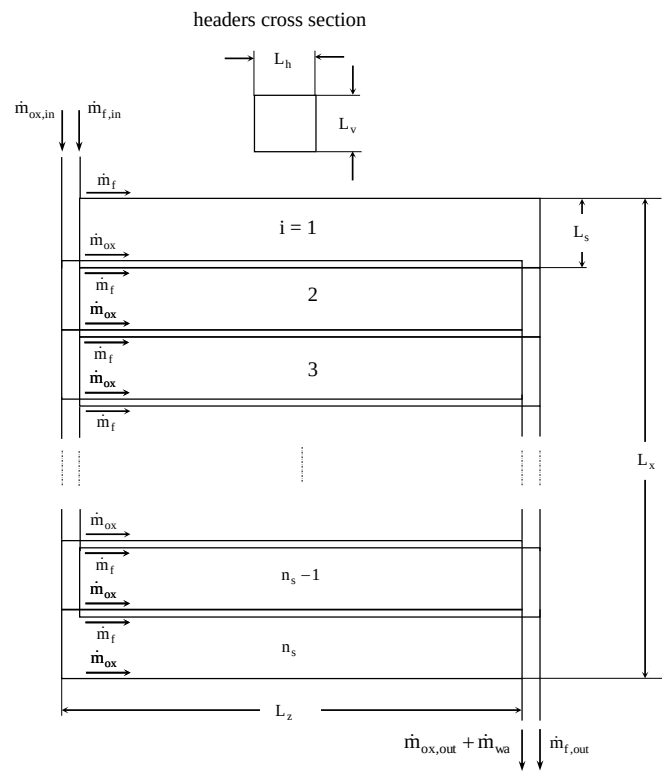

Figure 3 Flow structure sketch of headers and gas channels in the AMFC stack

where, $k = h_{f,in}, h_{ox,in}, h_{f,out}, h_{ox,out}$. The objective function defined by equation (22) depends on the internal structure and thickness of each individual cell, and on the external shape of the AMFC stack. The mathematical model allows for the computation of the total net power of the AMFC stack, $\widetilde{W}_{net}$. This is possible to achieve, once the physical values (Table 1) and a set of internal $(1 = 2\xi_b/\xi_s + \sum_{i=1}^{7}\xi_i/\xi_s \; e \; \xi_s)$ and external $(\xi_y/\xi_x \; e \; \xi_z/\xi_x)$ geometric parameters are selected for the overall system. The maximum theoretical efficiency of AMFC stack is given by:

$$\eta_i = \frac{\Delta\tilde{G}_3 + \Delta\tilde{G}_5}{\Delta\tilde{H}_3 + \Delta\tilde{H}_5} \quad (23)$$

The actual first-law efficiency of the fuel cell stack is:

$$\eta_I = E\frac{\widetilde{W}_s}{\Delta\tilde{H}_3 + \Delta\tilde{H}_5} \quad (24)$$

where, $E = V_{ref}I_{ref}/(\dot{m}_{ref}c_{p,f}T_\infty)$. The second-law efficiency is defined as the ratio between the actual electrical power and the reversible electrical power,

$$\eta_{II} = E\frac{\widetilde{W}_s}{\Delta\tilde{G}_3 + \Delta\tilde{G}_5} \quad (25)$$

The net efficiency of the AMFC stack is

$$\eta_{net} = E\frac{\tilde{W}_{net}}{n_s(\Delta\tilde{H}_3+\Delta\tilde{H}_5)} \quad (26)$$

Table 1 Physical properties used to obtain the numerical solutions

B = 0.156 [6]	R_{ox} = 0.2598 kJ/(kgK)
$c_{p,f}$ = 14.307 kJ/(kgK)	t_{ref} = 10^{-3} s
$c_{p,ox}$ = 0.918 kJ/(kgK)	T_f, T_{ox}, T_∞ = 298.15 K
$c_{v,f}$ = 10.183 kJ/(kgK)	U_{wi} = 50 W/(m^2K), i = 1,7
$c_{v,ox}$ =0.658 kJ/(kgK)	V_{ref} = 1V
I_{ref} = 1A	α_a = 0.76
k_f = 0.182 W/(mK)	α_c = 0.75
k_{ox} = 0.0267 w/(mK)	ζ_1, ζ_7 = 2
k_p = 0.1298 W/(mK)	μ_1 = 8.96 x 10^{-6} Pa.s
$k_{s,a}$ = $k_{s,c}$ = 0.1 W/(mK)	μ_7 = 20.7 x 10^{-6} Pa.s
k_{sol} = 0.571 W/(mK)	ρ_{sol} = 1406.39 kg/m^3
k_2, k_6 = 4.2 x 10^{-14} m^2 [7]	σ_{sol} = 53.2 Ω^{-1} m^{-1}
k_3, k_5 = 4.2 x 10^{-16} m^2 [7]	σ_1, σ_7 = 1.5×10^7 Ω^{-1} m^{-1}
p_f = 0.127 MPa	σ_2, σ_6 = 8570 1/Ωm
p_{ox} = 0.134 MPa	ϕ_2, ϕ_6 = 0.0085
p_∞ = 0.1 MPa	ϕ_3, ϕ_5 = 0.172
q = 2.5	ϕ_4 = 0.71
R_f = 4.157 kJ/(kgK)	

NUMERICAL METHOD

Equations (2), (4), (5), (6), (9), (10), and (11) formulate an initial value problem for dimensionless temperatures, along with initial conditions. Dimensionless pressures are calculated for CV2 and CV6 with two algebraic equations as discussed in the paragraphs right after Equation (6). The unknowns are θ_i and P_i, i.e., the temperatures of the seven control volumes, and the gas pressures at CV2 and CV6 outlets. Knowing the temperatures and pressures, it is possible to calculate the electric potential and the single and stack AMFC electrical and net power are calculated for any current level.

Two numerical methods were used. The first method calculates the transient behavior of the system, starting from a set of initial conditions, then the solution is marched in time (and checked for accuracy) until a steady state is achieved at any current level. The equations are integrated in time explicitly using an adaptive time step, 4th-5th order Runge-Kutta method [12]. The time step is adjusted automatically according to the local truncation error, which is kept below a specified tolerance of 10^{-6}. The second method is for the steady-state solution. The time derivatives are dropped from Equations (2), (4), (5), (6), (9), (10), and (11). The system reduces to seven nonlinear algebraic equations, in which the unknowns are the temperatures of the seven control volumes. This system is solved using a quasi-Newton method [12]. Convergence was achieved when the Euclidean norm of the residual of the system was less than 10^{-6}.

RESULTS AND DISCUSSION

In this section, the mathematical model is used to investigate the response of the prototype of the AMFC stack, the temperature distribution and pressure drop. In order to illustrate the application of the mathematical model of AMFC stack, numerical simulations are performed.

Figure 4 shows the polarization and net power curves obtained via simulation. The open circuit potential was equal to the reversible potential, since the mathematical model assumes that there are no losses due to species crossover between the two electrodes, and internal currents. Thus, the model allows for the separate verification of the contribution of the anodic and cathodic potential in the AMFC resulting potential. On the cathode side the oxygen reduction reaction occurs, which has a slower kinetics and higher overpotential losses than the anode, so the curves behave as expected, since they show that the cathodic potential is lower than the anodic potential. The behavior of the anodic potential curve indicates that potential losses due to charge transfer and diffusion are small, causing little anodic potential variation. It is also observed that the total AMFC stack power increases as current increases, although the power increase is not linear, and tends to be lower at higher currents.

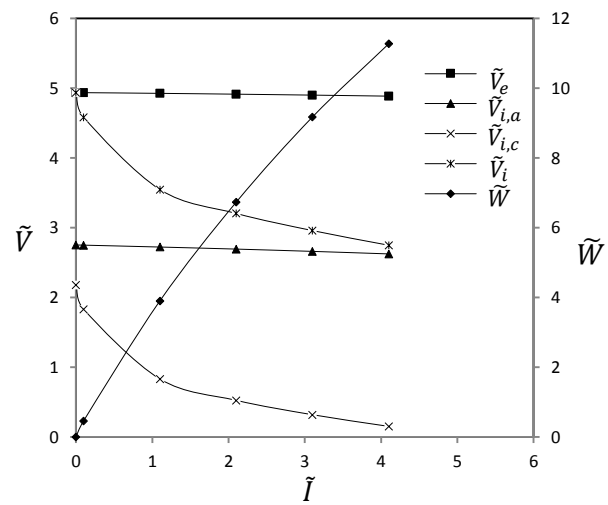

Figure 4 The AMFC stack polarization and power curves obtained numerically

Figure 5 shows the AMFC internal temperature distribution. It is seen that the temperature increases as current increases in steps $\Delta\tilde{I} = 0.5$ from $\tilde{I} = 0.1$. This is due to the heat generated by the electrochemical reactions and the potential loss (ohmic resistance and overpotentials - activation and diffusion). CV5 shows a slightly higher temperature than CV3. This is due to the fact that it is the control volume in which the oxygen reduction reaction occurs, which releases more heat than the hydrogen oxidation, which occurs in CV3. The simulation results show that the temperature spatial distribution in the AMFC stack is nonuniform. Therefore, the commonly used fuel cell uniform temperature distribution is only valid for small current conditions. The electrodes exchange current densities and other fuel cell parameters are temperature dependent, therefore the

uniform temperature assumption could lead to large errors when calculating the fuel cell steady state and dynamic response.

Figure 6 shows the power used to pump fluids through the AMFC stack headers as a function of current. The results show that the pumping power increases exponentially as current increases. This implies that the higher the working current in the stack, the greater the power loss due to pumping fluid through the headers. Although, quantitatively, such power loss could be different if the total mass flow rates in the stack headers were not distributed homogeneously to the single cells, qualitatively, the same effect on pumping power would be observed as current increased, and should be accounted for in any AMFC design.

Figure 7 shows the efficiency of the AMFC stack as a function of current. It is possible to observe that the ideal efficiency η_i hardly changes due to increasing current. The first-law of thermodynamics and total efficiencies, η_I and η_{net}, decrease as current increases. This decrease in efficiency is due to the increase of energy losses by diffusion, charge transfer, and ohmic overpotentials losses and losses due to increased fluid pumping power.

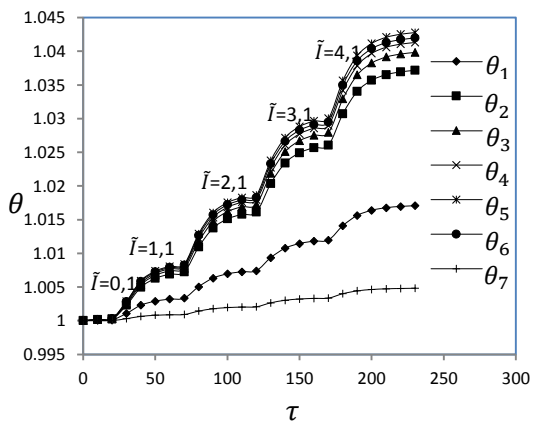

Figure 5 The thermal response of the AMFC stack obtained numerically

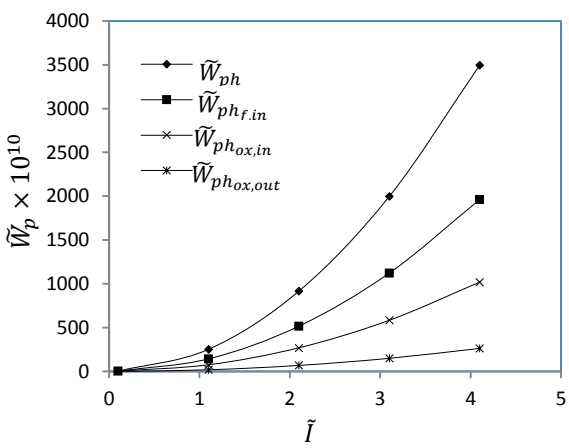

Figure 6 Pumping power consumption through the headers of the AMFC stack

CONCLUSIONS

In this work a dynamic mathematical model for an AMFC stack was developed, which considers the spatial dependence of temperature and pressure. The model is capable of assessing the AMFC stack polarization and power curves, and the pressure loss in the headers and cell gas channels. The proposed model needs to be validated experimentally, in order to be used reliably as an AMFC stack design, simulation, control and optimization tool.

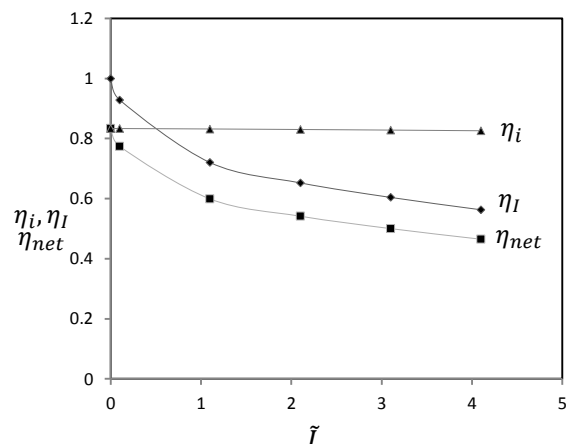

Figure 7 The AMFC stack efficiencies curves

REFERENCES

[1] Vargas, J.V.C., Bejan, A., Thermodynamic optimization of internal structure in a fuel cell, *International Journal of Energy Research*, Vol. 28, 2004, pp. 319-339.

[2] Mench, M.M., Wang, C., Thynell, S.T., An Introduction to Fuel Cells and Related Transport Phenomena, *International Journal of Transport Phenomena*, Vol. 3, 2001, pp.151-176.

[3] Young, J.B., Thermofluid modeling of fuel cells, *Annual Review of Fluid Mechanics*, Vol. 39, 2007, pp. 193-215.

[4] Ma, L., Ingham, D.B., Pourkashanian, M., Carcadea, E., Review of the Computational Fluid Dynamics modelling of fuel cells, *Journal of Fuel Cell Science and Technology*, Vol. 2, 2005, 246-257.

[5] Sommer, E.M., Martins, L.S., Vargas, J.V.C., Gardolinski, J.E.F.C., Ordonez, J.C., and Marino, C.E.B., Alkaline membrane fuel cell (AMFC) modelling and experimental validation, *Journal of Power Sources*, Vol. 213, 2012, pp. 16-30.

[6] Tarasevich, M.R., Sadkowski, A., Yeager, E., in: Convay, B.E., Bockris, J.O.M., Yeager, E., Khan, S.U.M., White R.E., (Eds.), Two-Dimensional Simulation of Direct Methanol Fuel Cell A New (Embedded) Type of Current Collector, *Comprehensive Treatise of Electrochemistry*, Vol. 7, 1983, pp. 310–398.

[7] Martins, L.S., Gardolinski, J.E.F.C., Vargas, J.V.C., Ordonez, J.C., Amico, S.C., Forte, M.M.C., The experimental validation of a simplified PEMFC simulation model for design and optimization purposes, *Applied Thermal Engineering*, Vol. 29, 2009, pp. 3036-3048.

[8] Ticianelli, E. A., *Eletroquímica: princípios e aplicações*. 2ª edição, Editora da Universidade de São Paulo, São Paulo, 2005.

[9] Vargas, J.V.C., Ordonez, J.C., Bejan, A., Constructual PEM fuel cell stack design, *International Journal of Heat and Mass Transfer*, Vol. 48, 2005, pp. 4410-4427.

[10] Shah R.K., London, A.L., *Laminar Flow Forced Convection in Ducts*, Academic Press, New York, 1978.
[11] Bejan, A., *Convection Heat Transfer*, 2ª ed., Wiley, New York, 1995.
[12] Kincaid, D., Cheney, D., *Numerical Analysis*, Wadsworth, Belmont, California, 1991.